




# Uranium Adsorption on Three Nanohydroxyapatites Under Various Biogeochemical Conditions

Precious Cooper · Jing Nie · Steven L. Larson · John H. Ballard · Heather M. Knotek-Smith · Ahmet Celik · Shaloam Dasari · Xianchun Zhu · Fengxiang X. Han 

Received: 2 June 2021 / Accepted: 5 August 2021 / Published online: 27 August 2021  
© The Author(s), under exclusive licence to Springer Nature Switzerland AG 2021

**Abstract** Uranium is a naturally occurring trace element and radionuclide. Uranium is introduced in the environment during industrial activities and nuclear energy accidents involving nuclear power plants, nuclear weapons tests, ore mining, and manufacturing, which may lead to the contamination of groundwater and soil. Hydroxyapatite (HAP) is a natural mineral with a high affinity for uranium in water. Groundwater often contains high carbonate concentrations that may affect uranium removal due to the formation of uranyl carbonate complexes. In order to understand the process of uranium removal, uranium adsorptions on three nano-HAPs were conducted under various biogeochemical conditions. Results showed that the fastest U adsorption occurred onto nano-HAP and U adsorption was strongly affected by biogeochemical conditions such as pH and the presence of carbonates, but less affected by temperature. The current study indicates that the presence of carbonates at pH's above the neutral range in groundwater may inhibit U removal with nanohydroxyapatites.

**Keywords** Hydroxyapatite · Carbonate · Uranium · Adsorption · pH effect

## 1 Introduction

Uranium is a naturally occurring trace element and radionuclide. Uranium (U) occurs in three isotopes, U-238, U-235, and U-234. Uranium is introduced to the environment anthropogenically as a result of industrial, military, and nuclear energy activities (Fuller et al., 2002; Zhou & Gu, 2005). Depleted uranium (DU) is a residuum of the uranium enrichment process with a majority of U as U-238, and a lower content of the fissile isotope U-235 than natural uranium U-235 is used as the fuel in nuclear reactors and in the manufacture of nuclear weapons. Large stocks of DU have been generated as a result of enrichment operations, especially in the USA (OECD/NEA, 2001). In recent years, the use of DU weapons such as DU containing penetrators has resulted in U contamination in soil and water on ranges (Kazery et al., 2021; Proctor et al., 2020; Zhang et al., 2020a). Uranium is often present in phosphate minerals leading to contamination of commercial products such as gypsum and P fertilizers (Kratz & Schnug, 2006). It was reported that the average U concentrations were found between 6 and 149 mg/kg U in P containing mineral fertilizers, while U in mineral fertilizers without P was below 1.3 mg/kg U (Kratz & Schnug, 2006).

---

P. Cooper · J. Nie · A. Celik · S. Dasari · X. Zhu · F. X. Han (✉)  
Department of Chemistry, Physics and Atmospheric Sciences, Jackson State University, Jackson, MS 39217, USA  
e-mail: Fengxiang.han@jsums.edu

S. L. Larson · J. H. Ballard · H. M. Knotek-Smith  
US Army Engineer Research and Development Center, Vicksburg, MS 39180-6199, USA

Uranium poses multiple health risks. Exposure to uranium can result in both chemical and radiological toxicities, but in most instances, chemical toxicity is of greater concern (Hartmann et al., 2010). Mechanisms of uranium toxicity have been suggested to include uranium interactions with phosphate groups on ATP and DNA. Renal uranium toxicity is the release of uranium from serum bicarbonate complex in the kidney to bind to available phosphate and protein, including uranium inhibition of mitochondrial ATPase activity and sodium transport mechanisms that can reduce the functionality and repair capacity of the epithelium (ATSDR, 2009; Keith et al., 2007).

The high affinity of uranium towards calcium phosphate minerals is exploited as a means of reducing uranium contamination in waters. Uranium phosphate minerals were shown to precipitate in uranium-contaminated water include autunite (AUT), sodium autunite, and chernikovite (CHN) minerals under favorable conditions (Zhang et al., 2020b). These cation and anion substitutions were  $\text{Ca}^{2+}$ ,  $\text{PO}_4^{3-}$ , and  $\text{CO}_3^{2-}$  (Fuller et al., 2002; Resende et al., 2006; Zhang et al., 2020b). Most recently, uranium was found to be bound by oxygen atoms in the phosphate and carbonyl groups, forming the specific nanopocket with high selectivity and high binding affinity of U (Yuan et al., 2020). The high binding affinity between U and P leads to in situ biomineralization of U to form highly stable and insoluble U mineral products in soils and sediments (Hartmann et al., 2010; Zhang et al., 2020b).

The mineral apatite and hydroxyapatites (HAP) have been extensively studied in the field in large systems and in the laboratory for removal of uranium. HAP consists of calcium, phosphates, and hydroxides and is ideal for easy and quick removal of U because it required no redox modifications (Lammers et al., 2017). It was reported that apatite as a multi-functional radionuclide sorbent effectively removed radionuclides (U, Sr, and, to some extent, Np, Am, Pu, and Co as well as  $\text{TcO}_4^-$  and  $\text{I}^-$ ) and other heavy metals by surface sorption, ion exchange, and surface precipitation and by providing phosphate to precipitate low-solubility minerals (Martin et al., 2008; Rigali et al., 2016). Processed natural apatites, artificial apatites, and functionalized composite apatites were prepared with high surface nanoapatite to remove U. Yang et al. (2017) reported an arginine modified hydroxyapatite carbon microsphere composites with

globular morphology and abundant functional groups to remove U(VI) from aqueous solutions. Arey et al. (1999) found that hydroxyapatite ( $\text{Ca}_5(\text{PO}_4)_3\text{OH}$ ) effectively immobilized U in two contaminated sediments with different organic carbon contents, lowering aqueous U to near proposed drinking water standards. The interactions of HAP and U(VI) occurred through two mechanisms: adsorption onto HAP and formation of U-P precipitation (Yang et al., 2017). Removal efficiencies greater than 99% have been shown in large-scale field experiments (Fuller et al., 2002).

The specific nature of the water environment such as pH, redox reactions, and complexation of other companion cations and anions as well as coexistence of humic acids has been shown to affect the effectiveness of sorption onto hydroxyapatite (Mehta et al., 2015). Identification of effective technologies for the collection of uranium from seawater has been a goal for researchers. Systems based on hydroxyapatite using hydroxyapatite have been shown to be limited due to the carbonate concentrations in seawaters. Stable precipitants  $(\text{UO}_2)(\text{PO}_4)_2$  and  $\text{CaUO}_2(\text{CO}_3)_2$  were shown to form in acid and neutral solutions, but less were formed in alkaline solutions (Krestou et al., 2004).

High concentration carbonate solutions have been shown to be effective for increasing the rate of uranium dissolution during the processing of uranium ore. When carbonates ( $\text{CO}_3^{2-}$ ,  $\text{HCO}_3^{2-}$ ) are present in uranium-containing waters, soluble uranium carbonate anions may be formed. The presence of these carbonates reduces the removal efficiency of uranium (Mehta et al., 2015; Gudavalli et al., 2018; Pan & Darvell, 2010). Solubility of calcium phosphates from HAP material increased in the presence of carbonate (Pan & Darvell, 2010). This suggests that precipitation of U-P phases might not be the mechanism for uranium uptake by HAP in use for permeable reactive barriers (Fuller et al., 2003). Another study with U-P phase showed that, at high bicarbonate, concentrations (25–100 mM) and pH values higher than 9 uranium release decreased from Ca-autunite. However, at lower concentrations of carbonate (0.5–3.0 mM) and lower pH of 7, the rate of uranium release increased (Gudavalli et al., 2018). This indicates the interaction of carbonate concentration and pH plays an important role in removing U from water.

In addition, carbonates formed uranium complexes with other cation and anion substitutions present in the groundwater (Mehta et al., 2014, 2015). U(VI) adsorption on goethite and soils was decreased due to formation of highly soluble, negatively charged U(VI) carbonates [ $\text{UO}_2(\text{CO}_3)^{2-}_2$  and  $\text{UO}_2(\text{CO}_3)^{4-}_3$ ] that did not strongly adsorb to soil surfaces (Duff & Amrhein, 1996). The presence of these complexes showed an increase of the uranium concentration in solution of uranium at pH values of 4.0 and 6.0 by < 10% in the absence of phosphate and less than 5% in the presence of phosphate (Lammers et al., 2017). Stewart et al. (2010) reported that U(VI) adsorption in natural and synthetic sediments decreased with formation of ternary uranyl – calcium – carbonate species.

Numerous studies have evaluated the interactions between uranium and low surface area biogenic apatites (Fuller et al., 2003; Zhang et al., 2020b). This study investigated the effect of biogeochemical conditions including carbonates, pH, and temperature on adsorption of U on three nanohydroxyapatites.

## 2 Materials and Methods

### 2.1 Hydroxyapatite Materials and Batch Sorption Experiments

Three different nanohydroxyapatites in the powder form were purchased from Sigma–Aldrich. They differed in surface areas, particle sizes, and U adsorption capacity (Table 1, discussed below). U(VI) stock solutions were prepared by dissolving uranyl nitrate hexahydrate in deionized water prepared in  $\text{CO}_2$ - and  $\text{CO}_2$ -free conditions accordingly. Carbonate concentrations were prepared by dissolving

sodium carbonate in  $\text{CO}_2$ -free deionized water to minimize interference when conducting the carbonate experiments.

Batch experiments were carried out to determine the effects of time, uranium concentrations, temperature, pH, and carbonate effects on U(VI) adsorption on three nanohydroxyapatites. Experiments were conducted in a closed 250-mL Erlenmeyer flask. The flasks contained a total of 25 mL and 1 g of HAP and were carried out in an agitated system. Then, 5 mL of the subsample was removed and centrifuged at 4500 rpm at 25 °C for 5 min. The remaining supernatant was filtered and analyzed by ICP-MS. All experiments were duplicated. Adsorption kinetics of U(VI) on HAPs was studied with 1.0 g HAP U(VI) and 10 mg/L U initial solutions. The mixtures were shaken on an agitated shaker at 0, 1, 2, 5, 10, 30, 60, 120, 240, and 1440 min. The samples were centrifuged and filtered. Then, U in the supernatants was analyzed with ICP-MS. U adsorption isotherm was studied with the initial uranium concentrations (0.5, 2, 10, 50, 100 mg/L). The mixtures were shaken for 1 h as determined by the previous kinetic experiment.

The biogeochemical conditions included pH, carbonates, and temperature. The influence of pH on the adsorption of U(VI) onto three different HAPs was examined. Different pH values of 1, 5.5, 7, 9.5, and 11 were adjusted with NaOH or HCl from the original pH of 100 mg/L U(VI) (approximately pH 3). The samples were then shaken for 1 h. Effects of carbonates on U adsorption were studied. Low and high carbonate concentrations of 2–100 mM were applied to 100 mg/L U(VI) solutions which were all prepared with  $\text{CO}_2$ -free water. The mixtures were shaken for 1 h. High carbonate concentrations of 100 mM were chosen to simulate a case with high alkalinity present in groundwater. This work proposed to mimic the results of uranium adsorption with HAP related to scenarios of field groundwaters. Four temperatures at 4, 25, 35, and 45 °C were examined to the effect of temperature on U adsorption where U was 100 mg/L.

XRD measurements were performed on the Mini-Flex 600 (Rigaku, Japan) with an 85 accelerated voltage of 45 kV and a current of 15 mA. Data were recorded in the range 86 of 10–80° with a step of 0.02° and speed of 5°/min. Fourier transform infrared spectra were collected on a Spectrum Two FT-IR 89 (PerkinElmer, USA), equipped with a deuterated

**Table 1** The surface areas, the maximum adsorption capacity ( $Q_m$  in mg/g), and affinity  $K$  of uranium adsorption on hydroxyapatites

	HAP1	HAP2	HAP3
$Q_m$ , mg/g	4.48	4.69	5.15
$K$ , L/mg	0.78	0.87	0.89
Surface area, $\text{m}^2/\text{g}$	1.79	96	22
Pore size, nm	2.27	1.56	2.05
Pore volume, $\text{cm}^3/\text{g}$	0.00054	0.0263	0.0055
Particle size, diameter	100–200 nm	0.5–1 $\mu\text{m}$	10–20 nm

tri-glycine sulfate (DTGS) detector. The surface areas of the materials were determined using BET analysis. Particle sizes were estimated with SEM.

### 3 Results and Discussion

#### 3.1 Characterization of Nanohydroxyapatites

Three nanohydroxyapatites had the similar XRD patterns (Fig. 1). However, HAP3 had sharp and intensive peaks compared to two other HAPs, indicating that HAP3 had a better crystalline structure. These XRD patterns were similar to the XRD patterns of standard hydroxyapatites from NIST (Ren et al., 2014). The five highest peaks were 31.77, 32.90, 32.18, 25.86, and 49.46 at  $2\theta^\circ$ , corresponding to hkl 211, 300, 112, 002, and 213, respectively (Grunenwald et al., 2014; Markovic et al., 2004; Ren et al., 2014). The samples with uranyl adsorbed on apatite surface under carbonate condition had the identical diffraction patterns with the original hydroxyapatites, and no diffraction peak shift was observed (data not shown). This was in agreement with the observation of Ren et al. (2014).

HAP 1 ( $\text{HCa}_5\text{O}_{13}\text{P}_3$ ) had a low surface area of  $1.79\text{ m}^2/\text{g}$  with a molecular weight of  $502.3\text{ g/mol}$  and a melting point of  $1100\text{ }^\circ\text{C}$  (Table 1). The sample contained both calcium hydroxyl phosphate and hydroxyapatite. HAP1 had a large particle size of  $10\text{--}20\text{ }\mu\text{m}$  (Fig. 2). HAP 2 was also a hydroxyapatite with an intermediate particle size with  $05\text{--}1.0\text{ }\mu\text{m}$  and  $96\text{ m}^2/\text{g}$  surface areas (Table 1, Fig. 2). HAP 3 ( $\text{HCa}_5\text{O}_{13}\text{P}_3$ ), a synthetic hydroxyapatite, had a

surface area of  $22\text{ m}^2/\text{g}$  and a small size of  $10\text{--}20\text{ nm}$  with a molecular weight of  $502.31\text{ g/mol}$  and melting point of  $1100\text{ }^\circ\text{C}$  (Table 1, Fig. 2). All three hydroxyapatites had surface area with the order:  $\text{HAP } 2 > \text{HAP } 3 > \text{HAP } 1$ .

FTIR results showed bands of the original HAP corresponding to the standard hydroxyapatites (Fig. 3). The FTIR of HAP1-3 spectrum only contains characteristic bands of phosphate and hydroxyl groups: (a) The bands at  $3572\text{ cm}^{-1}$ ,  $631\text{ cm}^{-1}$  arise from stretching and vibrational modes, of  $\text{OH}^-$  ions; (b) The  $1090\text{ cm}^{-1}$  and about  $1040\text{ cm}^{-1}$  bands arise from  $\nu_3\text{ PO}_4$ , the  $962\text{ cm}^{-1}$  band arises from  $\nu_1\text{ PO}_4$ , the  $601\text{ cm}^{-1}$  and  $574\text{ cm}^{-1}$  bands arise from  $\nu_4\text{ PO}_4$ . The sharpness of bands, especially the sharpness of the  $631\text{ cm}^{-1}$  and  $601\text{ cm}^{-1}$  bands, indicated a well-crystallized hydroxyapatite (Markovic et al., 2004; Slosarczyk et al., 2005). In compared three nanohydroxyapatites' FTIR, HAP3/HAP2 had more rich surface functional groups than HAP1.

#### 3.2 Adsorption Kinetics and Isotherms of U on Three Nanohydroxyapatites

Adsorption kinetic data showed that the U adsorption onto all 3 HAP was extremely rapid (Fig. 4). Within approximately 3 min, U was fully adsorbed onto HAP 1, 2, and 3. Longer reaction times did not significantly change the U adsorption on these nanohydroxyapatites. These results were consistent with previous observations that showed U adsorption equilibrium occurred between 1 and 2 h (Fuller et al., 2002; Krestou et al., 2004; Skwarek et al., 2019). Fast

**Fig. 1** XRD of nano-hydroxyapatites (HAP1, HAP2, and HAP3) samples

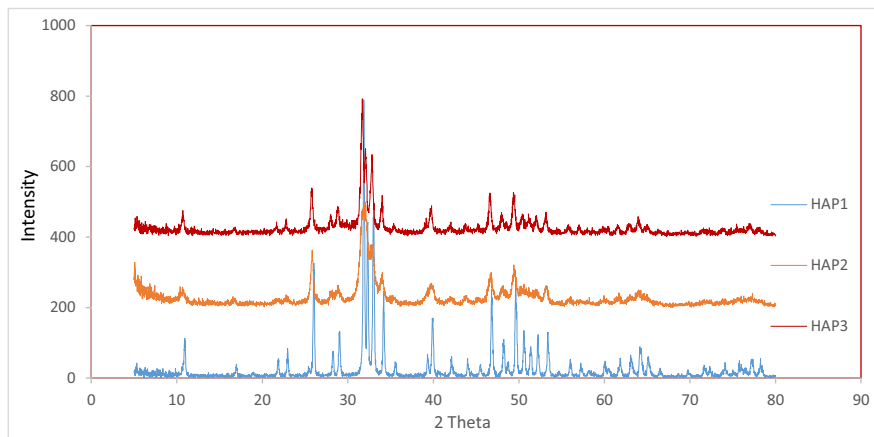
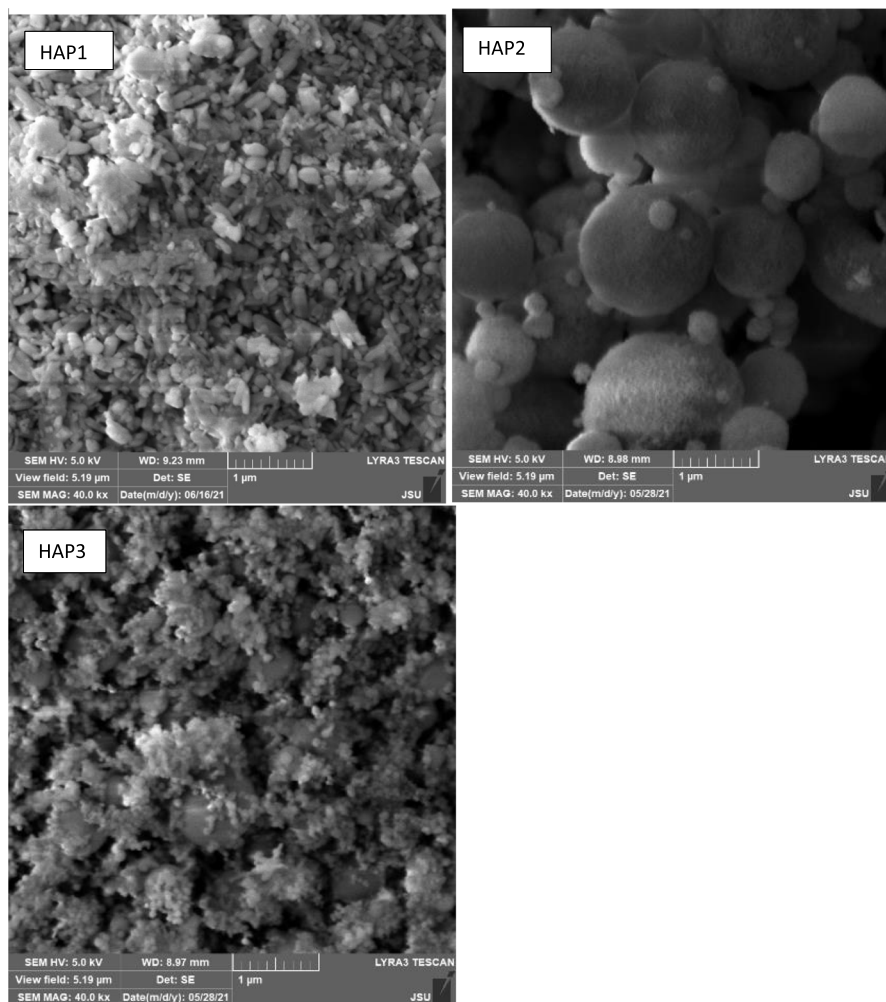


**Fig. 2** SEM of HAP1, 2, 3. The particle sizes of HAP1, 2, 3 were estimated as 100–200 nm, 0.5–1.0  $\mu\text{m}$ , and 10–20 nm, respectively. EDX indicated that the major elements were P and Ca and minor presence of Mg in these samples



adsorption of uranyl on nanohydroxyapatites indicates a potential for uranium removal from groundwater. The fast adsorption may be related with the relatively low surface area in these nanohydroxyapatites compared to other mesoporous materials with higher pore spaces and surface areas. A readily accessible surface makes for faster adsorption.

Three HAP materials showed maximum adsorption capacity of 4.48, 4.69, and 5.19 mg/g for HAP 1, 2, and 3, respectively (Fig. 5; Table 1). The adsorption processes on three HAPs were well described with a Langmuir model. The maximum U adsorption capacity among three HAPs are the following: HAP3 > HAP2 > HAP1. Both HAP 2 and HAP 3 had a higher surface area than HAP 1. The adsorption U on HAP3 was confirmed by FTIR with a weak peak around  $876\text{ cm}^{-1}$  from uranyl  $\nu_3$  mode (asymmetric

stretching) (Fig. 3) (Gorman-Lewis et al., 2008), but it was not observed in HAP1 and HAP2.

The possible mechanism of U adsorbed on surface of apatites may include precipitation as a formation of an amorphous or microcrystalline phase (Jeanjean et al., 1995). The XRD diffractograms did not indicate formation of other crystalline phase minerals after U adsorption. Formation of new crystalline phases and possible incorporation into the initial apatite was reported for Pb and intracrystalline diffusion and exchange were major mechanisms for Cd (Jeanjean et al., 1995). The addition of surface functional group significantly increased its adsorption of Pb. Wang et al. (2019) reported that esterified nanohydroxyapatite (n-HAP) had a high adsorption capacity of 2400 mg/g for Pb (II) in an acidic solution.

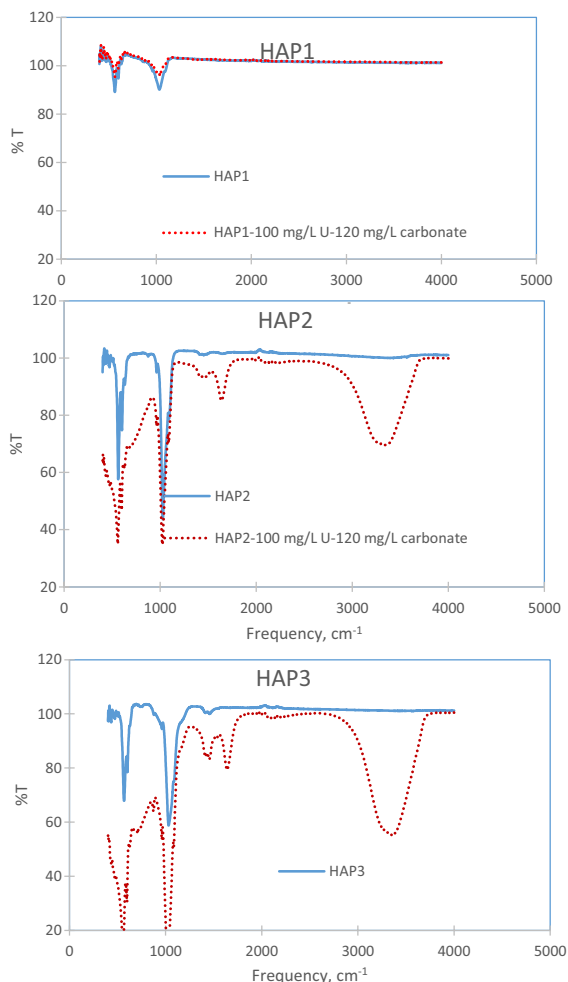


**Fig. 3** FTIR of HAP1-3 before and after adsorption of uranyl at 100 mg/L U under 2 mM (120 mg/L) carbonate (peaks: 598, 1023, 1463, 1635, and 3343  $\text{cm}^{-1}$ )

### 3.3 Biogeochemical Conditions Affecting the U Adsorption Processes

#### 3.3.1 pH Effects

U(VI) adsorption on HAP decreased with increasing pH (Fig. 6). However, pH effects on three hydroxyapatites were different. HAP1 was most sensitive to pH increase while HAP 3 was the least sensitive to pH changes. There was a significant decline ( $-55 \text{ mg/kg}$  per unit pH) in U adsorption as pH increased for HAP1 from 2500  $\text{mg/kg}$  at pH 1 to 1750 at pH 11. HAP2 had a slight decline ( $-12 \text{ mg/kg}$  per unit pH) with pH increased from 2463 at pH 1 to

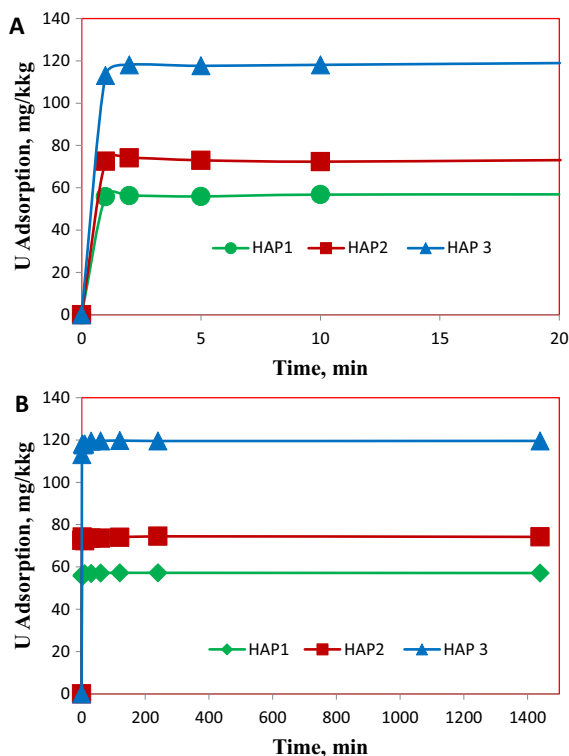


**Fig. 4** Kinetic of the adsorption of U(VI) on nano-HAP with an initial concentration of 10 mg/L at room temperature. **A** Kinetic experiment showing the initial contact time. **B** Kinetic experiment with a long-term adsorption

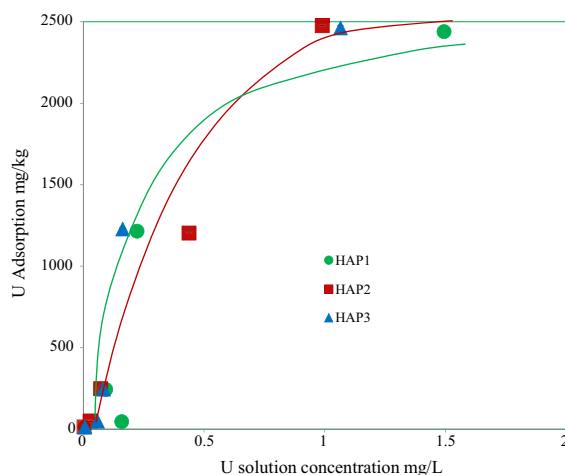


**Fig. 5** Adsorption isotherms of U onto 3 different nano-HAP materials

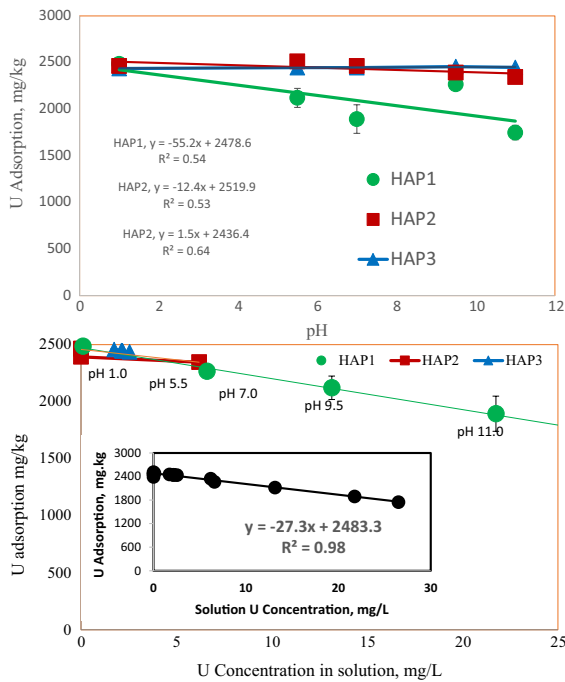


**Fig. 6** Effects of pH on U adsorption on three nano-hydroxyapatites. Upper: U adsorption on HAPs as a function of pH of solutions. Lower: U adsorption on HAPs as a function of U solution concentrations at specific pHs

2345 at pH 11, while HAP3 did not show significant change. This may be related to the richness of surface functional groups as shown in the FTIR (Fig. 3) spectra for HAP1. For HAP1 FTIR analysis showed fewer functional groups and BET analysis indicated low surface that could be affected by pH changes, while

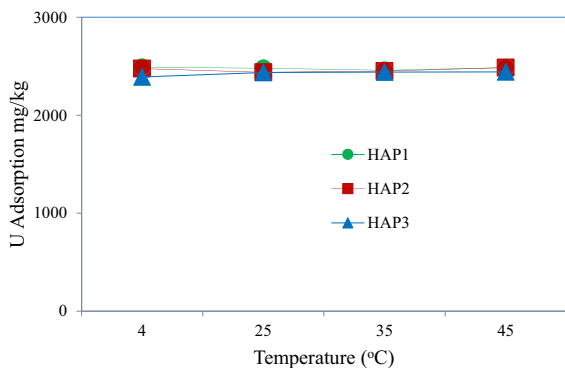


**Fig. 7** Temperature effect on the adsorption of 100 mg/L of U(VI) onto nano-HAPs

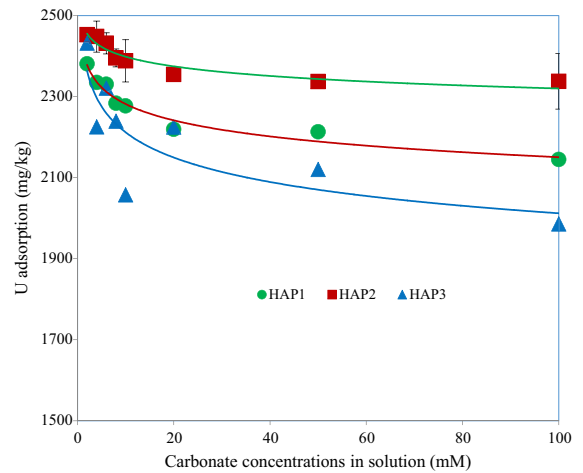


**Fig. 8** Effect of carbonate concentrations on adsorption of U on three nano-hydroxyapatites at 100 mg/L initial U(VI) at the room temperature

HAP3/HAP2 had rich functional groups and higher surface area.

The overall effects of pH on U adsorption on three nano-hydroxyapatites were in agreement with changing solubility of U (Fig. 6). With the increase of pH, the overall U solubility increased accordingly, resulting in the decrease in U adsorption on the solid surface of HAP. This may be related to the formation of hydroxyl and carbonate complexes of U in solutions at high pHs. These U complexes increased U solubility causing reduced adsorption on hydroxyapatite surface for U(VI). Above the pH of 6 uranium exists as carbonate complexes in the carbonate system (Fuller et al., 2003; Newsome et al., 2014; Soudek et al., 2011). In addition, it was reported that, when the pH levels were higher than 9, possible U precipitation may occur (Krestou et al., 2004). This was not observed in the present study with these nano-hydroxyapatites.

### 3.3.2 Effects of Temperature

Over a range of temperatures (4, 25, 35, 45 °C), no significant effect on uranium adsorption on nano-hydroxyapatites (Fig. 7) was observed. This study confirmed the previous observations that uranium adsorption was not dependent on temperature (Gudavalli et al., 2018). Similarly, uranium release by dissolution was reported to be independent of

**Table 2** A power model describing the effects of carbonate (mM) on U adsorption (mg/kg) on nanohydroxyapatites

Sample	Power model		Linear model		Logritherm model	
	Equation	$R^2$	Equation	$R^2$	Equation	$R^2$
HAP1	$y = 2420.8X^{-0.026}$	0.96	$y = -2.0X + 2322.1$	0.75	$y = -58.2 \ln(x) + 2416.6$	0.96
HAP2	$y = 2479.6X^{-0.014}$	0.90	$y = -1.1X + 2419.4$	0.58	$y = -34.6 \ln(x) + 2478.4$	0.90
HAP3	$y = 2431.4X^{-0.041}$	0.67	$y = -3.1X + 2277.2$	0.53	$y = -90.2 \ln(x) = 2423.6$	0.67

temperature with varying temperatures of 23–90 °C (Gudavalli et al., 2018).

### 3.3.3 Carbonate Effects

The presence of carbonates significantly decreased U(VI) adsorption on nano-HAP (Fig. 8, Table 2). This was especially true for HAP1 and HAP3. The reduction of adsorption in the presence of carbonate was not significant on U(VI) adsorption onto HAP2. The decrease in U adsorption due to the presence of carbonates could be modeled with a negative power equation ( $y = ax^{-b}$ , where  $y$  was U adsorption in mg/kg,  $a$  and  $b$  were constants, and  $x$  was the concentration of carbonates (Table 2). The initial low carbonate concentration (< 10 mM) significantly inhibited U adsorption on HAP almost in a negative linear way. With increase in carbonate concentrations, the inhibition effects became stabilized. Inhibition was greatest at low < 10–20 mM carbonate concentrations.

The interactions of uranium and HAP and uranium solubility were affected by carbonate. At lower concentration (2 mM), the FTIR spectral intensity did not change (Fig. 3). However, at a higher carbonate concentration of (100 mM), HAP 2 and HAP 3 showed new peaks at 867, 1417–1458  $\text{cm}^{-1}$  due to  $\text{CO}_3^{2-}$  and 3343  $\text{cm}^{-1}$  of  $\text{OH}^-$  stretching respectively (data not shown). FTIR peaks at 1417  $\text{cm}^{-1}$  and 874/876  $\text{cm}^{-1}$  (weak peak) were due to adsorbed  $\text{CO}_3^{2-}$  (Slosarczyk et al., 2005). This indicates that carbonates were adsorbed and present on the surface of HAP2 and HAP3 after adsorption of U under carbonate conditions. Peaks 1417  $\text{cm}^{-1}$  corresponded to the  $\nu_3$  mode (asymmetric stretching) of  $\text{CO}_3^{2-}$  and bands 874  $\text{cm}^{-1}$  were due to the  $\nu_2$  mode (out-of-plane bending) of  $\text{CO}_3^{2-}$  (Ren et al., 2014). Bands at 1455  $\text{cm}^{-1}$  were derived from  $\text{CO}_3^{2-}$  that replaced  $\text{OH}^-$  ions in the HA lattice (Markovic et al., 2004). Ren et al. (2014) pointed out the adsorbed carbonates on hydroxyapatite showed weak peaks at 875  $\text{cm}^{-1}$

( $\nu_2$ , out-of-plane bending) and  $\nu_3$  (asymmetric stretching) mode at 1419 and 1457  $\text{cm}^{-1}$ . The present study indicates that biogeochemical conditions such as pH and the presence of carbonates significantly affected U adsorption on nano-HAP. Low acidity and high concentrations of carbonates may increase U transport through soils.

## 4 Conclusion

In this study, batch experiments were conducted under various biogeochemical conditions to examine U adsorption isotherms and kinetics on three nanohydroxyapatites. The effects of carbonate and pH on U(VI) adsorption on HAPs were significant. The U(VI) adsorption process on HAP was fast and reached the plateau within 0.5 h. The presence of carbonate and high pH strongly inhibited U(VI) adsorption onto HAP due to potential formation of carbonate and hydroxide complexes, which increased U solubility in solution. This study suggests that nanohydroxyapatite was the ideal material for quick removal of uranium from groundwater, but the presence of carbonates and high pH will inhibit U removal from groundwater.

**Funding** This study was supported by the U.S. Army Engineer Research and Development Center (W912HZ-16-2-0021), the US Nuclear Regulatory Commission (NRC-HQ-84-16-G-0040, NRC-HQ-84-15-G-0042 and NRC-HQ-12-G-38-0038), and the US Department of Commerce (NOAA) (NA11SEC4810001-003499, NA16SEC4810009, NOAA Center for Coastal and Marine Ecosystems Grant # G634C22).

**Data Availability** The datasets generated during and/or analyzed during the current study are available from the corresponding author on reasonable request.



## References

- Arey, J. S., Seaman, J. C., & Bertsch, P. M. (1999). Immobilization of uranium in contaminated sediments by hydroxyapatite addition. *Environmental Science and Technology*, 33, 337–342.
- ATSDR (2009). Case Studies in Environmental Medicine (CSEM), Uranium toxicity, May 1, 2009. <https://www.atsdr.cdc.gov/csem/uranium/docs/uranium.pdf>. Accessed 1 Dec 2020.
- Duff, M. C., & Amrhein, C. (1996). Uranium(VI) Adsorption was reported on goethite and soil in carbonate solutions. *Soil Science Society of American Journal*, 60, 1393–1400.
- Fuller, C. C., Bargar, J. R., & Davis, J. A. (2003). Molecular-scale characterization of uranium sorption by bone apatite materials for a permeable reactive barrier demonstration. *Environmental Science and Technology*, 37(20), 4642–4649.
- Fuller, C. C., Bargar, J. R., Davis, J. A., & Piana, M. J. (2002). Mechanisms of uranium interactions with hydroxyapatite implications for groundwater remediation. *Environmental Science and Technology*, 36, 158–165.
- Gorman-Lewis, D., Skanthakumar, S., Jensen, M. P., Mekki, S., Nagy, K. L., & Soderholm, L. (2008). FTIR characterization of amorphous uranyl-silicates. *Chemical Geology*, 253(3–4), 136–140.
- Grunenwald, A., Keyser, C., Sautereau, A., Crubézy, E., Bertrand, L., & Drouet, C. (2014). Revisiting carbonate quantification in apatite (bio)minerals: A validated FTIR methodology. *Journal of Archaeological Science*, 49, 134–141.
- Gudavalli, R., Katsenovich, Y., & Wellman, D. (2018). Quantification of kinetic rate law parameters for the dissolution of natural autunite in the presence of aqueous bicarbonate ions at high concentrations. *Journal of Environmental Radioactivity*, 190–191, 1–9.
- Hartmann, H. M., Monette, F. A., & Avci, H. L. (2010). Overview of toxicity data and risk assessment methods for evaluating the chemical effects of depleted uranium compounds. *Human and Ecological Risk Assessment: An International Journal*, 6(5), 851–874.
- Jeanjean, J., Rouchaud, J. C., Tran, L., & Fedoroff, M. (1995). Sorption of uranium and other heavy metals on hydroxyapatite. *Journal of Radioanalytical and Nuclear Chemistry Letters*, 201, 529–539.
- Kazery, J. A., Proctor, G., Larson, S. L., Ballard, J. H., Knotek-Smith, H. M., Zhang, Q., Celik, A., Dasari, S., Islam, S. M., Tchounwou, P. B., & Han, F. X. (2021). Distribution and fractionation of uranium in weapon tested range soils. *American Chemical Society Earth and Space Chemistry*, 5(2), 356–364.
- Keith, L.S., Faroon, S.O.M., & Fowler, B.A. (2007). Uranium. In: *Handbook on the toxicology of metals* (3rd Ed, p 881–901). Academic Press.
- Kratz, S., & Schnug, E. (2006). Rock phosphates and P fertilizers as sources of U contamination in agricultural soils. In: Merkel B.J., Hasche-Berger A. (eds) *Uranium in the Environment*. Springer, Berlin, Heidelberg.
- Krestou, A., Xenidis, A., & Panias, D. (2004). Mechanism of aqueous uranium(VI) uptake by hydroxyapatite. *Minerals Engineering*, 17(3), 373–381.
- Lammers, L. N., Rasmussen, H., Adilman, D., deLemos, J. L., Zeeb, P., Larson, D. G., & Quicksall, A. N. (2017). Groundwater uranium stabilization by a metastable hydroxyapatite. *Applied Geochemistry*, 84, 105–113.
- Markovic, M., Fowler, B. O., & Tung, M. S. (2004). Preparation and comprehensive characterization of a calcium hydroxyapatite reference material. *Journal of Research of the National Institute of Standards and Technology*, 109, 553–568.
- Martin, W. A., Larson, S. L., Felt, D. R., & Wright, J. (2008). The effect of organics on lead sorption onto apatite II. *Applied Geochemistry*, 23, 34–43.
- Mehta, S. V., Maillot, F., Wang, Z., Catalano, G. J., & Giammar, E. D. (2014). Effect of co-solutes on the products and solubility of uranium (VI) precipitated with phosphate. *Chemical Geology*, 364, 66–75.
- Mehta, S. V., Maillot, F., Wang, Z., Catalano, G. J., & Giammar, E. D. (2015). Transport of U(VI) through sediments amended with phosphate to induce in situ uranium immobilization. *Water Research*, 69, 307–317.
- Newsome, L., Morris, K., & Llyod, R. J. (2014). The biogeochemistry and bioremediation of uranium and other priority radionuclide. *Chemical Geology*, 363, 164–184.
- OECD/NEA. (2001). Management of depleted uranium, nuclear development. *OECD Publishing*. <https://doi.org/10.1787/9789264294998-en>
- Pan, H., & Darvell, W. B. (2010). Effect of carbonate on hydroxyapatite solubility. *Crystal Growth & Design*, 10(2), 845–850.
- Proctor, G., Larson, S. L., Ballard, J. H., Knotek-smith, H., Waggoner, C., Uzn, R., Li, J., McComb, J., Jin, D., Arslan, Z., & Han, F. X. (2020). Rapid screening uranium in soils using portable X-ray fluorescence spectrometer, a comparative study. *ACS Earth & Space Chemistry*, 4(2), 211–217.
- Ren, F., Ding, Y., & Leng, Y. (2014). Infrared spectroscopic characterization of carbonated apatite: A combined experimental and computational study. *Journal of Biomedical Materials Research Part A*, 102A, 496–505.
- Resende, S. N., Nele, M., & Salim, M. M. V. (2006). Effects of anion substitution on the acid properties of hydroxyapatite. *Thermochimica Acta*, 451(1–2), 16–21.
- Rigali, M. J., Brady, P. V., & Moore, R. C. (2016). Radionuclide removal by apatite. *American Mineralogist*, 101(12), 2611–2619.
- Skwarek, E., Gładysz-Płaska, A., Choromańska, J. B., et al. (2019). Adsorption of uranium ions on nano-hydroxyapatite and modified by Ca and Ag ions. *Adsorption*, 25, 639–647.
- Slosarczyk, A., Paszkiewicz, Z., & Paluszkiwicz, C. (2005). FTIR and XRD evaluation of carbonated hydroxyapatite powders synthesized by wet methods. *Journal of Molecular Structure*, 744–747, 657–661.
- Soudek, P., Petrova, S., Benesova, D., Dvorakova, M., & Vanek, T. (2011). Uranium uptake by hydroponically cultivated crop plants. *Journal of Environmental Radioactivity*, 102(6), 598–604.

- Stewart, B. D., Mayes, M. A., & Fendorf, S. (2010). Impact of uranyl–calcium–carbonate complexes on uranium(VI) adsorption to synthetic and natural sediments. *Environmental Science and Technology*, *44*(3), 928–934.
- Wang, M., Zhang, K., Wu, M., Wu, Q., Liu, J., Yang, J., & Zhang, J. (2019). Unexpectedly high adsorption capacity of esterified hydroxyapatite for heavy metal removal. *Langmuir*, *35*(49), 16111–16119.
- Yang, D., Wang, X., Song, G., Zhao, G., Chen, Z., Yu, S., Gu, P., Wang, H., & Wang, X. (2017). One-pot synthesis of arginine modified hydroxyapatite carbonate microsphere composites for efficient removal of U(VI) from aqueous solutions. *Science Bulletin*, *62*, 1609–1618.
- Yuan, Y., Liu, T., Xiao, J., et al. (2020). DNA nano-pocket for ultra-selective uranyl extraction from seawater. *Nature Communication*, *11*, 5708.
- Zhang, D., Chen, X., Larson, S. L., Ballard, J. H., Knotek-Smith, H. M., Ding, D., Hu, N., & Han, F. X. (2020b). Uranium biomineralization with phosphate - biogeochemical process and its application. *American Chemical Society Earth and Space Chemistry*, *4*(12), 2205–2214.
- Zhang, Q., Larson, S. L., Ballard, J. H., Zhu, X., Knotek-Smith, H. M., & Han, F. X. (2020a). Uranium metal corrosion in soils with different soil moisture regimes. *Corrosion Science*, *179*, 109138.
- Zhou, P., & Gu, B. (2005). Extraction of oxidized and reduced forms of uranium from contaminated soils: Effects of carbonate concentration and pH. *Environmental Science & Technology*, *39*, 4435–4440.

**Publisher's Note** Springer Nature remains neutral with regard to jurisdictional claims in published maps and institutional affiliations.